Atmos. Chem. Phys., 21, 17995–18010, 2021
https://doi.org/10.5194/acp-21-17995-2021

Atmospheric Chemistry and Physics
Open Access
EGU

Measurement report: Fast photochemical production of peroxyacetyl nitrate (PAN) over the rural North China Plain during haze events in autumn

Yulu Qiu[1,2,3,4], Zhiqiang Ma[1,3,4], Ke Li[2], Mengyu Huang[5], Jiujiang Sheng[5], Ping Tian[5], Jia Zhu[2], Weiwei Pu[3,4], Yingxiao Tang[6], Tingting Han[3,4], Huaigang Zhou[3,4], and Hong Liao[2]

[1]Institute of Urban Meteorology, China Meteorological Administration, Beijing 100089, China
[2]Collaborative Innovation Center of Atmospheric Environment and Equipment Technology, Jiangsu Key Laboratory of Atmospheric Environment Monitoring and Pollution Control (AEMPC), School of Environmental Science and Engineering, Nanjing University of Information Science and Technology, Nanjing 210044, China
[3]Beijing Shangdianzi Regional Atmosphere Watch Station, Beijing 101507, China
[4]Environmental Meteorology Forecast Center of Beijing–Tianjin–Hebei, Beijing 100089, China
[5]Beijing Weather Modification Office, Beijing 100089, China
[6]Tianjin Environmental Meteorology Center, Tianjin 300074, China

Correspondence: Zhiqiang Ma (zqma@ium.cn)

Received: 29 April 2021 – Discussion started: 23 June 2021
Revised: 4 November 2021 – Accepted: 5 November 2021 – Published: 9 December 2021

Abstract. Photochemical pollution over the North China Plain (NCP) is attracting much concern. We usually view peroxyacetyl nitrate (PAN) as the second most important photochemical pollutant featuring high mixing ratios during warm seasons. Our observations at a background site in the NCP identified high PAN concentrations, even during haze events in autumn. The substantial increasing ratios of PAN, by 244 % and 178 %, over the morning hours (08:00–12:00 local time) on 20 and 25 October 2020 were 10.6 and 7.7 times larger than those on clean days. Polluted days are characterized by higher temperature, higher humidity, and anomalous southerly winds compared with clean days. Enhanced local photochemistry has been identified as being the dominant factor that controls the PAN increase in the morning at the rural site, as the time when prevailing wind turns to a southerly wind is too late to promote direct transport of PAN from the polluted urban region. By removing the effect of direct transport of PAN, we provide a quantitative assessment of net PAN chemical production rate of 0.45 ppb h^{-1} for the mornings of polluted days, also demonstrating the strong local photochemistry. Using observations and calculated photolysis rates, we find that acetaldehyde oxidation by hydroxyl radical (OH) is the primary pathway of peroxyacetyl radical formation at the rural site. Acetaldehyde concentrations and production rates of HO_x ($HO_x = OH + HO_2$) on polluted days are 2.8 and 2 times as large as those on clean days, leading to a remarkable increase in PAN in the morning. Formaldehyde (HCHO) photolysis dominates the daytime HO_x production, thus contributing to fast photochemistry of PAN. Our observational results suggest the cause of a rapid increase in PAN during haze events in autumn at a rural site of the NCP and provide evidence of important role of HCHO photolysis in secondary pollutants at lower nitrogen oxide emissions. This highlights the urgency of carrying out strict volatile organic compound controls over the NCP during the cold season and not just in summer.

1 Introduction

Since the late 1960s, peroxyacetyl nitrate (PAN) has been identified as being a key photochemical pollutant in the atmosphere, having adverse effects on human health and vegetation (Heuss and Glasson, 1968; Taylor, 1969). It is a sec-

ondary pollutant formed through reactions between peroxyacetyl radical ($CH_3C(O)O_2$; PA) and nitrogen dioxide (NO_2; Xue et al., 2014). The dominant three pathways of PA formation are through oxidation of acetaldehyde (CH_3CHO), photolysis of acetone ($CH_3C(O)CH_3$), and methylglyoxal (CH_3COCHO; MGLY), as follows (Fischer et al., 2014):

$$CH_3CHO + OH \xrightarrow{O_2} PA + H_2O \quad (R1)$$

$$CH_3C(O)CH_3 + h\nu \xrightarrow{O_2} PA + CH_3 \quad (R2)$$

$$CH_3COCHO + h\nu \xrightarrow{O_2} PA + HCO. \quad (R3)$$

PAN can be thermally decomposed back to PA and NO_2, which is the major removal pathway in the lower troposphere, as follows:

$$PAN \leftrightarrow PA + NO_2. \quad (R4)$$

PAN's precursors, such as CH_3CHO, acetone, and MGLY, are usually viewed as the second-generation precursors because they not only directly come from anthropogenic emissions but are also the oxidation products of various nonmethane hydrocarbons (NMHCs; Xue et al., 2014). These NMHCs are first-generation precursors. Thus, photochemical production of PAN could be largely determined by the oxidation of volatile organic compounds (VOCs) with radicals in the presence of nitrogen oxide ($NO_x = NO + NO_2$). During the daytime, the hydroxyl (OH) radical is usually considered as being the primary oxidant in the troposphere. Nitrous acid (HONO), mainly generated from direct traffic emissions and the heterogeneous conversion of NO_2 on ground and aerosol surfaces (Xue et al., 2020; Liu et al., 2021), is a key source of OH radicals in the early morning (Alicke et al., 2003) and on cold days (Hendrick et al., 2014; Kim et al., 2014; Lu et al., 2019). In addition, the photolysis of carbonyls may also greatly influence HO_x ($HO_x = OH + HO_2$) and ozone (O_3) production at lower NO_x concentrations during cold seasons (Edwards et al., 2014; Li et al., 2021). For example, Li et al. (2021) found that HO_x radicals from photolysis of formaldehyde (HCHO) accelerated the ozone upsurge during COVID-19 in Beijing in response to substantial NO_x reductions.

The North China Plain (NCP) region is now experiencing urbanization and industrial expansion, leading to air pollution as a matter of intense debate. Since 2013, the Chinese government has performed strict emission reduction measures, and this has resulted in rapid decrease in the $PM_{2.5}$ concentration (Zhai et al., 2019). However, increases in O_3 concentrations in the NCP region have frequently been reported, owing to the large amounts of anthropogenic precursor emissions and meteorological variability so far (Ma et al., 2016; Li et al., 2020; Lu et al., 2020; Dang et al., 2021). Li et al. (2020) reported that the maximum 8 h average (MDA8) O_3 concentrations in summer NCP during 2013–2019 were increased by a rate of 3.3 ppb a^{-1}. As another important photochemical pollutant, PAN pollution events were also extensively recognized in both the urban (Zhang et al., 2014, 2015, 2017; Y. Qiu et al., 2019a) and rural NCP regions (Y. Qiu et al., 2020b; Wei et al., 2020) at the same time. These also confirm the severity and complexity of photochemical pollution in this highly populated NCP region.

Compared with the relatively low concentration of O_3 in the autumn and winter seasons (Wang et al., 2013), PAN pollution events are also observed on cold days over the NCP (Zhang et al., 2014; Liu et al., 2018; Zhang et al., 2019; G. Zhang et al., 2020; Y. Qiu et al., 2019b, 2020a), which is associated with particulate pollution events. For example, Y. Qiu et al. (2020a) reported a high PAN level of 4.13 ppb (parts per billion) during the COVID-19 lockdown period of January–February 2020 in Beijing, and the average value was 52 % higher than that in summer 2019 when solar radiation was intensive. A common explanation for the observed high PAN concentration in winter is its susceptibility to be accumulated under a stable atmosphere and regional transport due to decreased thermal decomposition under low temperatures (Y. Qiu et al., 2019b; G. Zhang et al., 2020). Moreover, accelerated photochemistry can also play a role during PAN pollution events on cold days (Zhang et al., 2014; Liu et al., 2018; Y. Qiu et al., 2020b; G. Zhang et al., 2020) since unexpectedly high PAN concentrations are usually observed during the daytime. Thus, PAN could represent a key indicator of photochemistry on cold days.

Despite several field campaigns and experiment analysis in recent years, the fast PAN formation mechanisms during autumn and winter over the NCP region have still not been fully explored so far, especially over clean rural regions. Previously, HONO photolysis was tentatively considered as being the cause of strengthened local photochemistry in the winter of the urban NCP region, thus contributing to increases in PAN concentrations (Liu et al., 2018; J. Zhang et al., 2020). For example, Liu et al. (2018) found a positive relationship between HONO and PAN in winter over an urban site of the NCP, thus highlighting the importance of HONO in faster PAN formation during haze episodes. By conducting sensitivity simulations using the Weather Research and Forecasting model with online coupled chemistry (WRF-Chem), J. Zhang et al. (2020) reported that HONO photolysis could result in PAN increases of 80 %–150 % in eastern China during polluted days in winter. However, these studies neglect the impact of carbonyl photolysis that allows for fast photochemistry and may play a dominant role in PAN formation over the rural region with low NO_x emissions. The lack of an integrated observation of VOCs, HONO, and other related chemical species in previous studies hinders the comprehensive understanding of PAN chemistry.

Here, we show observational evidence of fast PAN formation at a rural site on the NCP during haze events in autumn 2020. The dominant contribution from enhanced local photochemistry to PAN concentration increases is verified by an analysis between variations in wind and PAN concentrations,

along with quantitative assessment of direct physical transport utilizing carbon monoxide (CO) as a tracer. Using simultaneous observations of PAN, VOCs, HONO, and photolysis rates, we calculate the daytime HO_x production rates and reveal the contributions of precursors and radical oxidants in daytime PAN increases. Our results suggest the cause of the rapid PAN increase over the rural NCP, and provide a new insight into assessing the impacts of high reactive VOCs from urban plumes on the atmospheric oxidation capacity and secondary pollutant formation over the rural NCP.

2 Experiments and methods

2.1 Site

We conduct the field campaign at the Shangdianzi (SDZ) National Atmospheric Background Station, which is near the northern border of Beijing, China (40.65° N, 117.17° E, 293.9 m a.s.l.), about 100 km northeast of the urban center (Fig. 1). The SDZ site is a World Meteorological Organization (WMO)/Global Atmosphere Watch (GAW) background station in northern China, which has the representation of air pollutants in rural NCP. The sampling site is located on the roof of the station, approximately 6 m from the ground. The prevailing wind at night and in the morning is northeasterly and turns to southwesterly in the afternoon due to effect of the local valley wind. The SDZ site is upwind of the polluted NCP region and is surrounded by extensive vegetation and sparsely populated small villages. The mean $PM_{2.5}$ concentration in 2020 at the SDZ site is 26 $\mu g\,m^{-3}$, which is much lower than the present air quality standard in China (35 $\mu g\,m^{-3}$). An integrated observation experiment was performed at the SDZ site from 13 to 27 October 2020, including measurements of PAN, VOCs, O_3, HONO, NO_x, CO, and photolysis rates. At the same time, we also performed PAN observations at an urban site in Beijing, located on the campus of the Minzu University of China (39.95° N, 116.32° E). The urban site is between the second and third ring roads in downtown Beijing and is mainly affected by traffic and residential sources.

2.2 Instruments and measurements

The details of the instruments used in this study have been summarized in Table S1. PAN is measured with an online gas chromatograph equipped with an electron capture detector (GC-ECD). The capillary column is mounted in a compact temperature-controlled oven for which the temperature is fixed at 12 °C. The ECD temperature is maintained at 50 °C ±0.2 °C. The PAN instrument has a time resolution of 5 min, with a detection limit of 20 ppt (parts per trillion). More information about the configuration of this instrument has been presented in our previous work (Y. Qiu et al., 2020b). To calibrate the GC-ECD instrument, PAN is produced throughout the reactions between a calibrated NO flow (1 ppm – parts per million; Linde plc, SPECTRA Environmental Gases) and the 285 nm photolysis of excess acetone. The reaction yield of PAN is 93 %. A regular multiple-point calibration check (PAN concentrations of 1, 2, and 4 ppb) has been conducted every month to guarantee the quality of the PAN results since August 2015, usually on a day characterized by persistent northerly winds with low PAN concentrations.

We use the proton transfer reaction time-of-flight mass spectrometer (PTR-ToF-MS) to measure the concentrations of formaldehyde, acetaldehyde, acetone, propene, and isoprene. The ambient air is pumped into a cabin with a flow rate of 15 L min^{-1} through a 3 m long Teflon tube. We use a Teflon membrane filter to remove the particles in the airflow. Then the air is evolved into a reaction drift tube of PTR-ToF-MS through a 1/16 in. (1,58 mm) PEEK tubing inlet. We set the drift tube at 60 °C, 2.2 mbar and 600 V. H_3O^+ is used as the primary reaction ion, as it has been widely used in analyzing trace gases. The measurement has a time resolution of 5 min. A gas calibration unit (GCU-a; GCU-advanced v2.0) is used to perform the zero air generation and PTR-ToF-MS calibration, which is also produced from the PTR-ToF-MS manufacturer, i.e., Ionicon Analytik GmbH. A VOC scrubber catalyst is installed in the GCU-a unit and heated to 350 °C, thus producing VOC-free zero air by passing ambient air through it. We use a dynamic dilution of the multicomponent gas standard (Apel Riemer Environmental Inc., USA) to calibrate the PTR-ToF-MS every month, including formaldehyde, acetaldehyde, acetone, propene, and isoprene of 1 ppm ±5 %. Detailed descriptions of the PTR-ToF-MS configuration and calibration methods are listed in Sheng et al. (2018).

HONO measurements are carried out using a long-path absorption photometer (LOPAP-03; QUMA Elektronik & Analytik GmbH). The HONO gas is collected in the atmosphere and then absorbed by the solutions. The sampling rates of gas flow and liquid flow are set to 1.3 L min^{-1} and 0.30–0.34 mL min^{-1}, respectively. We used a known concentration of nitrous acid standard solution to calibrate the LOPAP instrument every week to guarantee data quality. All of the observation data can be accessed from Qiu and Ma (2021). Besides, we also carried out zero measurements every day, lasting 1 h, during the observation period.

Online measurements of O_3, NO_x, $PM_{2.5}$, and CO are also conducted using a UV photometric O_3 analyzer (model 49i; Thermo Electron Corporation, USA), a NO_x analyzer (model 42i; Thermo Electron Corporation, USA), a TEOM-1405 (tapered element oscillating microbalance) analyzer, and a cavity ring-down spectrometer (G2401; Picarro, Inc., USA), respectively. It is noteworthy that parts of PAN could be considered as being NO_2 because of the disadvantage of the model 42i analyzer. Photolysis rates (J), including $J_{O(^1D)}$, J_{HCHO}, and J_{HONO}, are simultaneously measured by the PFS-100 photolysis rate analyzer (Focused Photonics Inc., China). The analyzer receives solar radiation with a quartz probe and transfers the radiation to the spectrum via

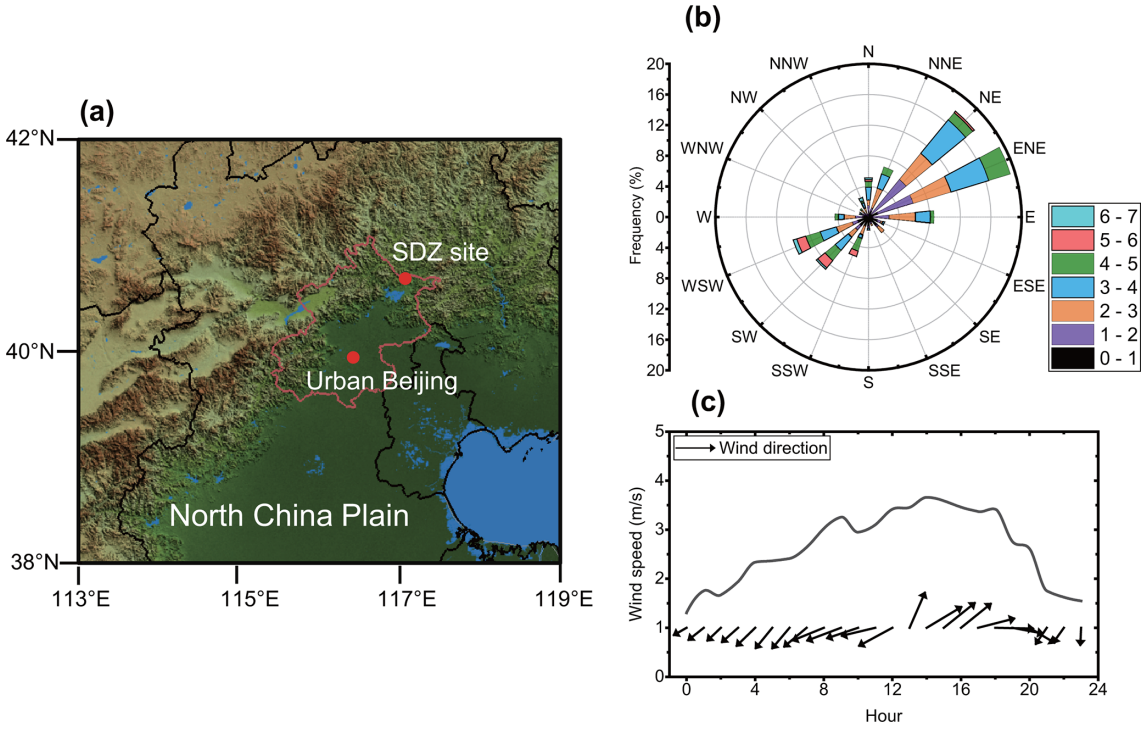

Figure 1. **(a)** Locations of the SDZ site, urban Beijing, and North China Plain. **(b)** Averaged wind frequencies (percent) and **(c)** diurnal wind variations during the observation period at the SDZ site.

optical quartz fibers. The spectrum data are evaluated and compared with reference data, via a mathematical approach, to obtain the photolytic rate.

2.3 Other data

As the SDZ site is also a national meteorology observatory, meteorological variables, including temperature (T), relative humidity (RH), sea level pressure (SLP), and wind direction and speed, were continuously measured during the observation period. The hourly European Centre for Medium-Range Weather Forecasts Reanalysis v5 (ERA5) data ($0.25° \times 0.25°$), accessed from https://cds.climate.copernicus.eu/ (last access: 1 December 2020), are used to assess the impact of atmospheric circulation on pollutant levels. Concentrations of odd oxygen ($O_x = O_3 + NO_2$) obtained from the Beijing Municipal Ecological and Environmental Monitoring Center (http://www.bjmemc.com.cn/, last access: 6 December 2020) are also utilized. Here, we average the mixing ratios over eight stations in the urban region and at the Miyunshuiku (MY) site to represent the O_x levels in urban region and rural region near SDZ, respectively.

3 Results

3.1 High PAN levels during haze events in autumn

Figure 2a shows the temporal variations in PAN and the related atmospheric components at the SDZ site from 13 to 27 October 2020. The mean concentrations of PAN, $PM_{2.5}$, O_3, NO_x, HCHO, HONO, CH_3CHO, and C_3H_6 are 1.11 ± 0.88 ppb, $34.2 \pm 23.8\ \mu g\ m^{-3}$, 27.6 ± 14.5 ppb, 8.5 ± 2.8 ppb, 4.9 ± 3.9 ppb, 0.15 ± 0.16 ppb, 1.6 ± 1.1 ppb, and 0.7 ± 0.5 ppb, respectively. Compared with recent studies in China (Table S2), the observed PAN concentration at the SDZ site is generally lower than 1.5–1.89 ppb over the urban NCP (Zhang et al., 2017; Liu et al., 2018) and 2.05 ppb in urban southwestern China (Sun et al., 2020), comparable to 0.93–1.04 ppb in the suburban NCP region (Y. Qiu et al., 2019a; Zhang et al., 2019). But it is remarkably higher than several observations from southern China, with PAN levels of 0.55–0.63 ppb (Zhu et al., 2018; L. Zeng et al., 2019; Hu et al., 2020) and 0.36–0.44 ppb in Tibet (Xu et al., 2018), implying a severe photochemical pollution level over the NCP on a regional scale.

As shown in Fig. 2a, two pollution events (20 and 25–26 October) occurred at the SDZ site, with hourly PAN concentrations in excess of 3 ppb. Meanwhile, daytime O_3 concentrations during the two pollution episodes were 16 %–39 % higher than those on clean days (Table 1). A similar increase was also found in $PM_{2.5}$, which was strongly cor-

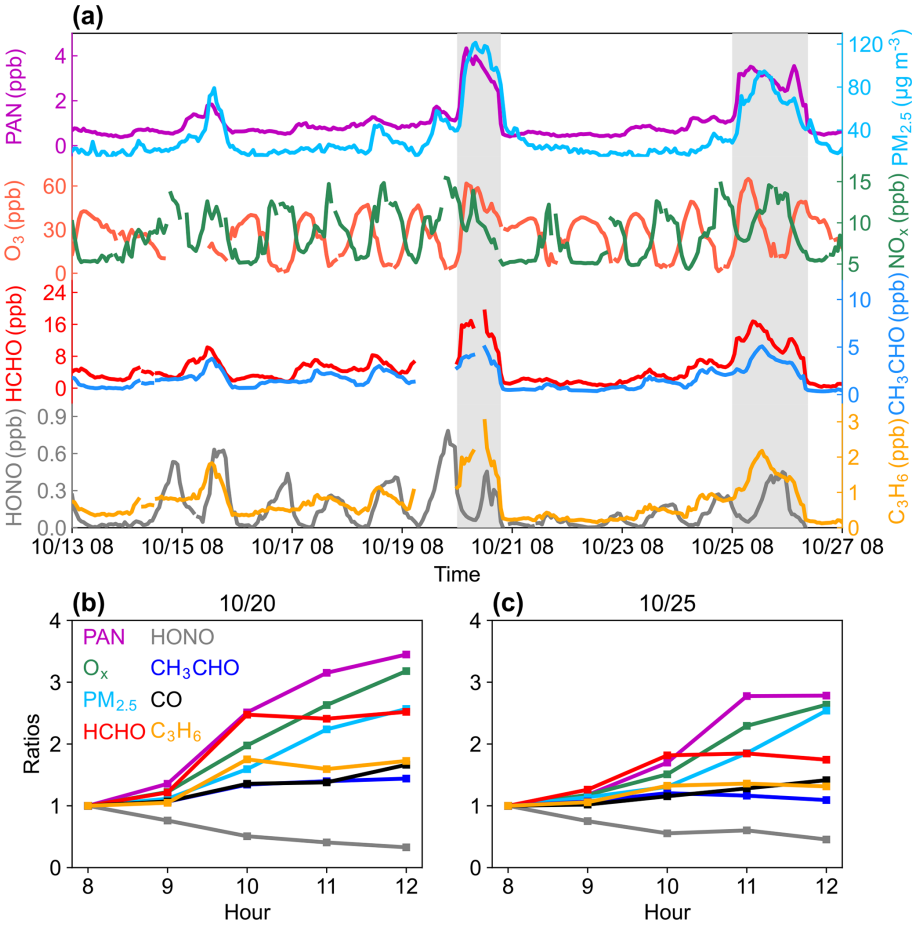

Figure 2. (a) Observed hourly concentrations of PAN (ppb), $PM_{2.5}$ (micrograms per cubic meter; hereafter $\mu g\,m^{-3}$), O_3 (ppb), NO_x (ppb), HCHO (ppb), CH_3CHO (ppb), HONO (ppb), and C_3H_6 (ppb) at the SDZ site from 13 to 27 October 2020. The shades denote the days when hourly PAN concentrations exceeded 3 ppb. **(b, c)** Ratios of atmospheric constituent concentrations to the concentrations at 08:00 LT (local time), in the morning on 20 and 25 October, when substantial PAN growths took place.

related with PAN, with a correlation coefficient (R) of 0.9 during the observation period. Daily mean NO_x concentrations on polluted days were 16 %–42 % higher than clean days, as shown in Table 1, implying the potential role of regional transport under unfavorable meteorological conditions. Substantial increases in PAN and related pollutants could be identified in the mornings on 20 and 25 October. Figure 2b and c display the ratios of individual component concentrations to their concentrations at 08:00 LT on the 2 polluted days. In general, PAN concentrations exhibited fast growth ratios by 244 % and 178 % during the morning hours (08:00–12:00 LT) of 20 and 25 October, which were 10.6 and 7.7 times larger than those during clean days. These increase rates are highest among all species illustrated in Fig. 2b and c. The corresponding growth ratios of 9 %–44 % for PAN's primary precursor, CH_3CHO, and 41 %–66 % for chemically inert CO are much lower than PAN. This result suggests the potential enhanced local photochemistry at the SDZ site on polluted days during autumn.

Previous studies also reported synchronous increases in PAN and $PM_{2.5}$ during cold seasons over the NCP region (Liu et al., 2018; Zhang et al., 2019). For example, Zhang et al. (2019) showed that the PAN concentration doubled at noon during a haze episode at a suburban site in Beijing, in comparison to that in the morning, together with synchronous increases in $PM_{2.5}$ and O_3. Liu et al. (2018) also reported rapid growth of PAN during a wintertime pollution event in urban Jinan, along with high $PM_{2.5}$ concentration; however, they showed rather low O_3 concentration during winter haze days because of high NO_x concentrations and intense NO titration effects in the urban region. Therefore, synchronous increases in PAN and $PM_{2.5}$ can take place in the whole NCP region during cold days, while the co-occurrence of O_3 increases may just exist in suburban and background regions where NO_x emissions are rather low.

Table 1. Statistical results of concentrations for PAN (ppb), $PM_{2.5}$ ($\mu g\,m^{-3}$), O_3 (ppb), NO_x (ppb), HCHO (ppb), CH_3CHO (ppb), C_3H_6 (ppb), and HONO (ppb), on average, during clean days and polluted days. The clean days represent the time that excludes the polluted days (20 and 25–26 October), and the daytime denotes 08:00–19:00 LT.

Species	Mean	Clean	Polluted		
			20 Oct	25 Oct	26 Oct
PAN (ppb)	1.11 ± 0.88	0.77 ± 0.35	2.67 ± 1.17	2.33 ± 1.06	2.09 ± 1.06
Daytime PAN	1.22 ± 0.99	0.79 ± 0.25	3.41 ± 0.95	2.85 ± 0.85	2.17 ± 1.07
O_3 (ppb)	27.6 ± 14.5	26.2 ± 12.2	34.6 ± 22.2	31.8 ± 22.5	31.0 ± 14.0
Daytime O_3	36.1 ± 11.5	33.7 ± 8.4	46.7 ± 17.9	46.8 ± 18.0	39.1 ± 10.9
$PM_{2.5}$ ($\mu g\,m^{-3}$)	34.2 ± 23.8	25.7 ± 12.9	81.5 ± 33.2	57.2 ± 25.7	57.2 ± 18.5
NO_x (ppb)	8.47 ± 2.80	7.93 ± 2.54	11.3 ± 2.31	10.8 ± 4.35	9.24 ± 3.58
HCHO (ppb)	4.86 ± 3.88	3.63 ± 2.19	14.1 ± 3.67	10.9 ± 4.35	7.21 ± 4.62
CH_3CHO (ppb)	1.61 ± 1.09	1.31 ± 0.75	3.87 ± 0.61	3.09 ± 1.09	2.26 ± 1.45
C_3H_6 (ppb)	0.70 ± 0.50	0.56 ± 0.33	1.94 ± 0.49	1.28 ± 0.52	0.94 ± 0.62
HONO (ppb)	0.15 ± 0.16	0.13 ± 0.14	0.34 ± 0.25	0.17 ± 0.09	0.25 ± 0.17

3.2 Meteorological conditions

On a synoptic scale, PAN levels are largely influenced by meteorological conditions. Figure 3 shows the atmospheric circulation during clean days and 2 polluted days (20 and 25 October), focusing on variations in sea level pressure and wind in the boundary layer. During the observation period, the SDZ site was affected by a high-pressure system in the west associated with northwesterly wind in the upper boundary layer. A similar weather pattern was also identified on clean days, facilitating pollutant diffusion. During the 2 polluted days, southwesterly winds prevailed over the NCP. On 20 October, the SDZ site was to the south of a strong low-pressure system, leading to southwesterly winds arising from pressure gradient force. The southwesterly winds on 25 October were caused by a weak high-pressure system with an anticyclone in the southeast. As the observation site is located north of the urban region, the prevailing southwesterly winds could promote pollution transport from downtown Beijing to the rural site.

Temporal variations in the observed meteorological variables at the SDZ site are shown in Fig. 4a–e. The daytime T, RH, SLP, $J_{O(^1D)}$, and meridional wind (V) near the surface are also compared between clean days and polluted days and illustrated as box plots in Fig. 4f–j. Here, positive V values denote southerly winds, while negatives represent northerly winds. We find positive daytime T and RH anomalies on 20 and 25 October, indicating hot and wet weather conditions compared with clean days. Although higher temperature can promote the thermal decomposition of PAN, it also accelerates photochemistry, thus increasing the PAN levels. Higher RH has been proved to inhibit heterogeneous reactions of PAN on soot, leading to increases in the PAN concentration in the atmosphere (Zhao et al., 2017). Negative SLP anomalies and positive V anomalies on 20 and 25 October could contribute to pollution accumulation and transport to the north, coinciding with the ERA5 results shown in Fig. 3. As shown in Fig. 4j, daytime $J_{O(^1D)}$ on 20 and 25 October was $3.1 \times 10^{-6}\,s^{-1}$ and $4.3 \times 10^{-6}\,s^{-1}$, respectively, which was 47 % and 26 %, respectively, lower than that on clean days ($5.8 \times 10^{-6}\,s^{-1}$). These reductions are likely to result from aerosol and cloud radiative effects, which are unfavorable for photochemical reactions. Consequently, the meteorological conditions during pollution events are favorable for the accumulation and transport of PAN and its precursors, as well as promoting chemical formation due to relatively higher temperature and RH compared with clean days, though reductions in photolysis rates are identified.

3.3 Strong local photochemistry at the SDZ site

As the SDZ site is a clean background station with scarce anthropogenic sources, the substantial increases in PAN and other secondary pollutants on 20 and 25 October were tentatively supposed to be related to pollutant transport from the urban region. However, these increases on polluted days are impossibly caused by direct PAN transport from the urban region despite its relatively long thermal lifetime during the observation period ($\sim$ 1 d). Here, direct PAN transport refers to PAN itself, excluding its precursors. Figure 5a–c show the temporal variations in daytime PAN and O_x at the urban, SDZ, and MY site on the 2 polluted days when abrupt increases in PAN take place. Detailed locations of the three sites and distances between them are shown in Fig. 5d. Southerly wind facilitates pollutant transport from the urban region to the SDZ site, while the northerly wind brings relatively clean air. On 20 October, the PAN concentrations at the SDZ site rose from 1.3 ppb at 08:00 LT to 4.3 ppb at 12:00 LT. However, the wind did not turn to southerly until 10:00 LT (Fig. 5a). The calculated transport distance was just about 26 km during 10:00 to 12:00 LT, as the observed southerly wind speed was 1.2–3.4 $m\,s^{-1}$. It is approximately the dis-

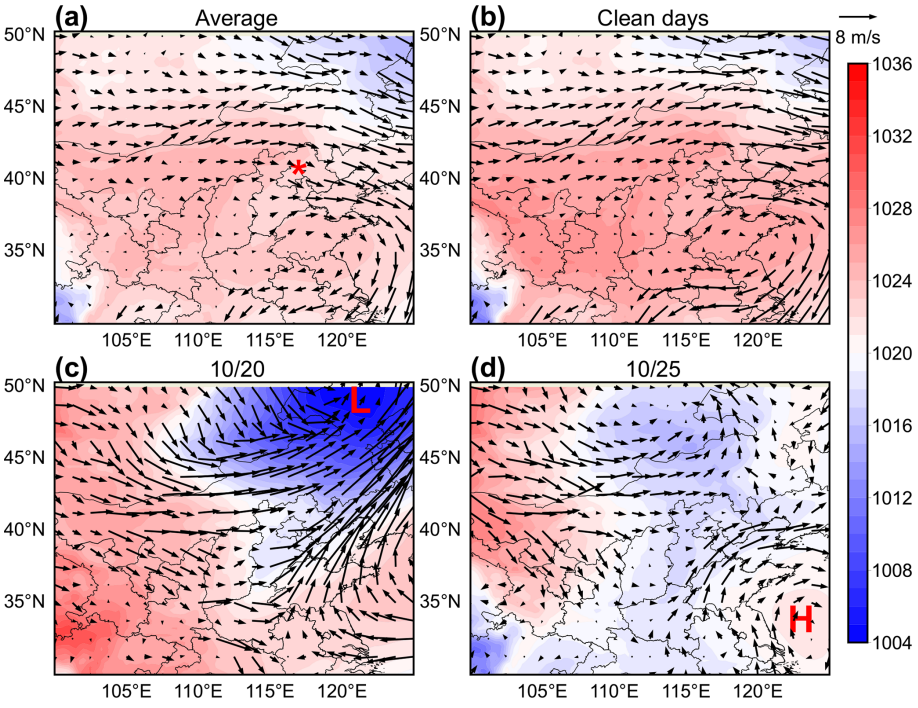

Figure 3. Winds at 925 hPa and sea level pressure (hectopascals) derived from ERA5 data **(a)** averaged during 13–27 October, **(b)** clean days (13–19 and 21–24 October), and on **(c)** 20 October and **(d)** 25 October. The red asterisk in panel **(a)** shows the location of the SDZ site.

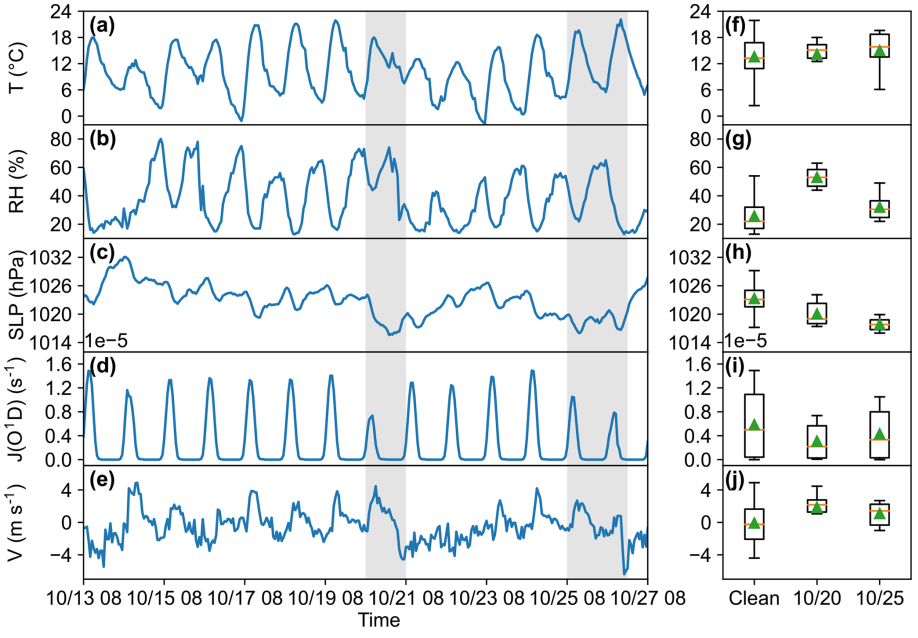

Figure 4. (a–e) Time series of observed temperature (T; degrees Celsius), relative humidity (RH; percent), sea level pressure (SLP; hectopascals), photolysis rate for O_3 ($J_{O(^1D)}$; per second), and meridional wind (V; meters per second) during 13–27 October at the SDZ site. The shades denote the polluted days. **(f–j)** Box plots for daytime meteorological parameters during clean days (13–19 and 21–24 October) and 2 polluted days. The red lines and green triangles denote the median and mean values, respectively.

tance between the SDZ site and the MY site, which is another rural site near the Miyun Reservoir (Fig. 5d). The O_x concentration at the MY site from 09:00 to 12:00 LT on 20 October was slightly lower than that at the SDZ site (Fig. 5c), indicating the similar photochemical pollution levels between the two sites. Therefore, the substantial increase in PAN in the morning on 20 October was not likely driven by direct PAN regional transport, despite the observed high PAN concentration at the urban site (Fig. 5a). On another pollution day (25 October), the prevailing wind turned southerly after 12:00 LT. Direct PAN transport from the urban region could not explain the fast PAN growth in the morning. Moreover, PAN increases in the morning resulting from the planetary boundary layer evolution are deemed to be unlikely because our previous observation at an urban site in the NCP region has reported that nighttime PAN concentration in autumn of 2018 in the upper boundary layer was just 9.5 % higher than the surface layer PAN concentration (Y. Qiu et al., 2019a). The slightly higher PAN concentration in upper layer could not be the cause of rapid increases in PAN in the mornings on polluted days.

As shown in Fig. 2b and c, the rates of increase in PAN during polluted days at the SDZ site are much larger than CO. It is known that CO is chemically inert and served as an ideal tracer for anthropogenic sources, which can represent transport processes from pollution sources well (Gao et al., 2005; Worden et al., 2013; Chen et al., 2020). Thus, further evidence of enhanced photochemistry during the pollution episodes comes from the quantitative assessment of direct PAN transport and chemical production, using CO as a tracer. Ambient PAN concentration is affected by physical processes (such as regional transport) and local photochemical formation. Thus, the change rate of PAN at the SDZ site ($\frac{\mathrm{d[PAN]}}{\mathrm{d}t}$) is the sum of net chemical production rate ($\frac{\mathrm{d[Chem]}}{\mathrm{d}t}$) and the change due to physical processes ($\frac{\mathrm{d[Phys]}}{\mathrm{d}t}$).

$$\frac{\mathrm{d[PAN]}}{\mathrm{d}t} = \frac{\mathrm{d[Chem]}}{\mathrm{d}t} + \frac{\mathrm{d[Phys]}}{\mathrm{d}t}. \quad (1)$$

As there are no intense anthropogenic sources along the transport from downtown Beijing to the SDZ site, we assume that PAN / CO ratios remain constant along the transport pathway, and the PAN change rate at the SDZ site, due to direct physical transport ($\frac{\mathrm{d[Phys]}}{\mathrm{d}t}$), is identical to that of CO ($\frac{\mathrm{d[CO]}}{\mathrm{d}t}$).

$$\frac{\mathrm{d[Phys]}}{\mathrm{d}t} = \frac{\mathrm{d[CO]}}{\mathrm{d}t} \times \frac{\mathrm{[PAN]}}{\mathrm{[CO]}}. \quad (2)$$

The net chemical production rate ($\frac{\mathrm{d[Chem]}}{\mathrm{d}t}$) is the sum of chemical production (P[PAN]) and the thermal decomposition (Eq. 3). The thermal decomposition rate (L[PAN]) can be calculated as $-k$[PAN], where the chemical reaction rate coefficient k is temperature dependent (Seinfeld and Pandis, 2006). Therefore, the chemical production of PAN (P[PAN]) can be derived from the difference between the net chemical production rate ($\frac{\mathrm{d[Chem]}}{\mathrm{d}t}$) and the chemical decomposition rate, as shown in Eq. (4).

$$\frac{\mathrm{d[Chem]}}{\mathrm{d}t} = P\,\mathrm{[PAN]} - k\mathrm{[PAN]} \quad (3)$$

$$P\,\mathrm{[PAN]} = \frac{\mathrm{d[PAN]}}{\mathrm{d}t} - \frac{\mathrm{d[CO]}}{\mathrm{d}t} \times \frac{\mathrm{[PAN]}}{\mathrm{[CO]}} + k\mathrm{[PAN]}. \quad (4)$$

We use 4 h as dt and separate a day into the morning (08:00–12:00 LT), afternoon (12:00–16:00 LT), evening (16:00–20:00 LT), and night (20:00–08:00 LT). It should be noted that the assumption of a constant PAN / CO ratio along the transport pathway may lead to the underestimation of physical impacts, especially in the afternoon when temperature is high. Therefore, the change rates due to chemical processes calculated by PAN / CO method are the maximum values that are possible.

Figure 6 displays the process diagnostic results of PAN at the SDZ site. Here, we define the PAN change rates induced by chemical processes and physical processes as Chem and Phys, respectively. A positive PAN change rate (Chem + Phys) was only found in the morning (08:00–12:00 LT), which was attributed to high net chemical production rate (Chem) of 0.14 ppb h^{-1}. In the afternoon (12:00–16:00 LT) and evening (16:00–20:00 LT), regional transport (Phys) by southwesterly winds contributed to increases in PAN with rates of 0.05 and 0.02 ppb h^{-1}, respectively. However, the negative net chemical production rates (-0.07 and -0.06 ppb h^{-1}) originating from large thermal loss rates (L[PAN], -0.57 and -0.34 ppb h^{-1}) completely overcome the PAN increases from transport. This evidence manifests as a local photochemical formation of PAN in the morning, coinciding with PAN's diurnal variation. The impacts of photochemistry and regional transport on PAN were both largely strengthened during polluted days (Figs. 6 and S1). The net chemical formation rate (Chem) was 0.45 ppb h^{-1} in the mornings of polluted days, which was 6.3 times as large as that on clean days. This again demonstrates that strong local photochemical reactions contribute most to PAN enhancement in the mornings on the 2 polluted days, rather than direct transport.

3.4 Impacts of precursors on rapid increase of PAN

A key question in explaining the substantial increase in PAN at the SDZ site is how its precursors change. PAN is directly formed through the reaction between PA radical and NO_2. As NO_2 is much more abundant than PAN in the atmosphere, PA formation through VOC oxidation and photolysis may have greater impacts on PAN. As noted above, the dominant three pathways of PA formation are through direct oxidation of CH_3CHO, photolysis of acetone, and methylglyoxal (MGLY; Fischer et al., 2014). Figure 7 displays the calculated PA production rates through these three VOC species. The PA production through CH_3CHO+OH

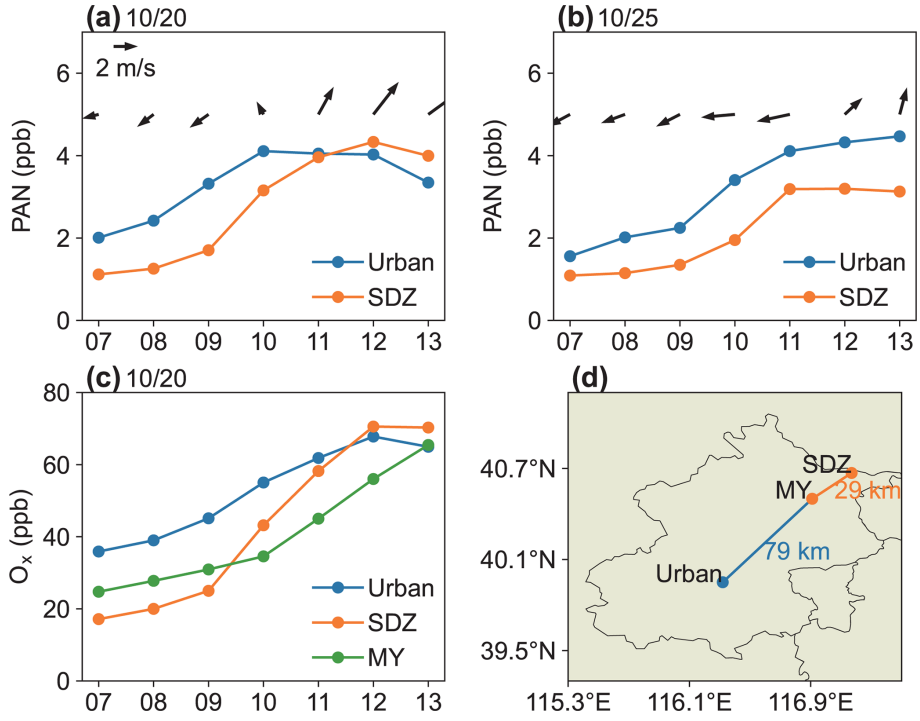

Figure 5. Hourly variations in PAN concentrations (ppb) and surface wind at the urban and SDZ site during 07:00–13:00 LT on **(a)** 20 October and **(b)** 25 October. **(c)** Hourly variations in O_x concentrations (ppb) at the urban, SDZ, and MY site during 07:00–13:00 LT on 20 October. **(d)** Detailed locations of the urban, SDZ, and MY site and the distances between them.

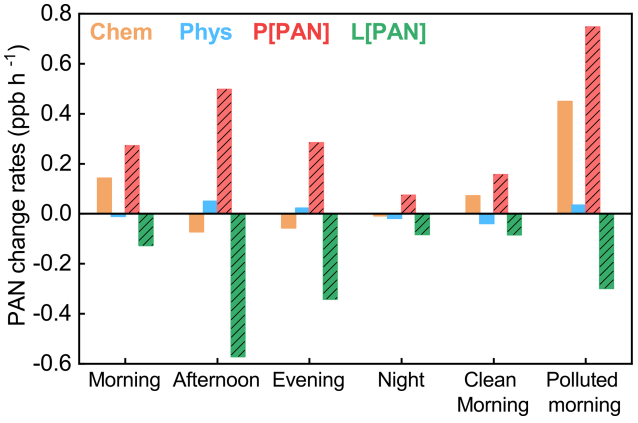

Figure 6. Process diagnostic analysis of PAN on average and in the morning on clean and polluted days. Chem, Phys, P[PAN], and L[PAN] denote the net chemical production, physical changes, chemical production, and loss rates of PAN, respectively. Morning, afternoon, evening, and night correspond to 08:00–12:00, 12:00–16:00, 16:00–20:00, and 20:00–08:00 LT, respectively.

is calculated by $k \times [CH_3CHO] \times [OH]$, where $k = 5.55 \times 10^{-12} \times \exp(311/T)$ (Seinfeld and Pandis, 2006), and the CH_3CHO concentration is obtained from PTR-ToF-MS measurements, while the OH concentration is assumed to be with a maximum value of 3.0×10^6 molec. cm^{-3} at noon, which is consistent with Lu et al. (2019). The PA production rates through the photolysis of acetone and MGLY are calculated by $J_{acetone} \times$ [acetone] and $J_{MGLY} \times$ [MGLY], where the photolysis rates (J) are estimated using the tropospheric ultraviolet and visible radiation (TUV) model described in Madronich and Flocke (1999). The acetone concentration is collected from PTR-ToF-MS measurements, and the MGLY concentration is obtained from X. Qiu et al. (2020), who found the modified modeling MGLY concentration near the SDZ site in autumn of 2018 to be about 0.012 ppb. Moreover, we also calculate the contribution from the oxidation of MGLY by OH to PA production using $k \times$ [MGLY] $\times$ [OH]. As seen in Fig. 7, CH_3CHO oxidation by the OH radical plays a dominant role in PA production at the SDZ site. The relatively lower photolysis rate of acetone ($\sim 10^{-7}$ s^{-1}) and previously reported low MGLY concentration ($\sim$ 0.012 ppb) in autumn at the rural site (X. Qiu et al., 2020) inhibit high PA production rates through these two species. Although methacrolein (MACR) and methyl vinyl ketone (MVK), two oxidation products of isoprene and monoterpene, also contribute to PA production through photolysis (Liu et al., 2010; Fischer et al., 2014), the observed low concentration (average of 0.12 ppb) in autumn resulted in a noontime PA production rate of about 5500 molec. cm^{-3} s^{-1}. This is even lower than the PA production rate from acetone photolysis. Our results are consistent with previous studies, which have also confirmed the dominant role of $CH_3CHO + OH$ in PA formation during winter in urban Beijing (Xu et al., 2021), over eastern

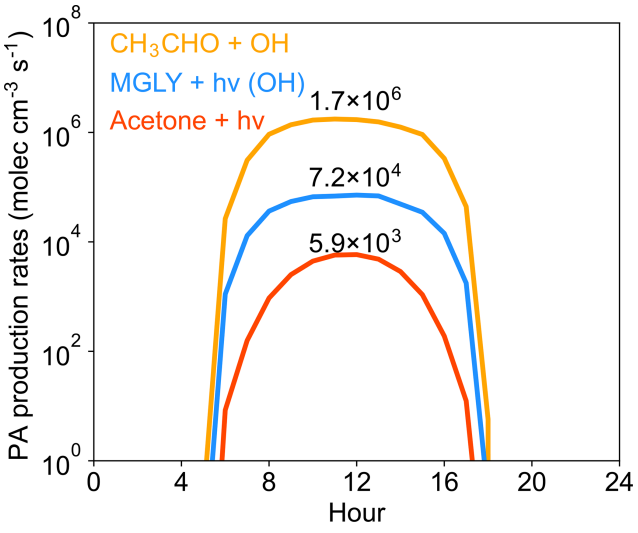

Figure 7. Estimated variations in daytime PA production rates (molecules per cubic centimeter per second; hereafter molec. cm^{-3} s^{-1}) through CH_3CHO, acetone, and MGLY, averaged during the observation period at the SDZ site. The numbers on the top of the lines denote the maximum values at noon through the three pathways.

China (L. Zeng et al., 2019; J. Zhang et al., 2020), and even on global scale (Fischer et al., 2014).

The calculation of PA production rates by CH_3CHO and OH can also help us to estimate the PA concentration if we suppose that PA radicals can reach a steady state. Thus, we can also obtain PAN production rates by the product of reaction coefficient, PA, and NO_2 concentrations (Method S2). Using this method, the calculated mean PAN production rate in the morning was 0.25 ppb h^{-1} and increased to about 0.6 ppb h^{-1} on polluted days (Fig. S2). Although these values are slightly lower than those estimated by the PAN / CO method (0.27 and 0.73 ppb h^{-1}) shown in Fig. 6, the comparable PAN production rates using two different methods also suggest the presence of enhanced photochemistry during polluted days.

CH_3CHO could be directly emitted to the atmosphere and also formed through the oxidation of alkenes, such as C_3H_6. Figure 8 shows the daily variations in CH_3CHO and C_3H_6 concentrations at the SDZ site during episode 1 (16–20 October) and episode 2 (22–26 October). Here, we use the daily concentrations at 08:00 LT to represent the VOC level before the daytime active photochemistry. On 16 October, the NCP region was influenced by a high-pressure system with northerly winds (Fig. 4e), which was conducive to pollutant diffusion. From 17 to 20 October, persistent stagnant conditions with southerly winds during the late morning to evening contributed to pollutant accumulation and transport from the urban region to the SDZ site, though northerly winds prevailed from night to morning. Thus, the C_3H_6 and CH_3CHO concentrations at the SDZ site during 16 to 20 October both exhibited increasing trends, thus reflecting the cumulative effect. This is similar in appearance to that episode from 22 to 25 October (Fig. 8d and e), during which the C_3H_6 and CH_3CHO concentrations increased by 180 % and 196 %, respectively. These values indicate that the cumulative effect under persistent stagnant weather conditions increased VOC concentration levels before strong photochemistry occurred in the morning on 20 and 25 October. Furthermore, high PAN / NO_2 ratios on 20 and 25 October, when rapid increases in PAN occurred (Fig. 8c, f, i), also enabled the identification of strong photochemistry with a relatively high precursor level. As illustrated in Fig. 6, the net chemical formation rate in the morning on the polluted days was 6.3 times larger than that on clean days. However, the increase ratios for CH_3CHO and C_3H_6 were just about 2.8 times as large as that on clean days (Fig. 8g and h). That is to say, increases in VOC concentrations could not fully explain the remarkable increase in PAN, although it indeed promoted the photochemical formation of PAN during the two pollution events.

3.5 Impacts of radicals on rapid increase of PAN

In addition to VOC precursors, the observed strengthened chemical formation in the mornings on polluted days could also relate to increased OH concentration and atmospheric oxidation capacity. The photolysis of HONO, HCHO, and O_3 can provide a major source of HO_x radicals (Schnell et al., 2009; Edwards et al., 2014; Tan et al., 2018; Li et al., 2021). Here, the calculated time series of HO_x production through the photolysis of HONO, HCHO, and O_3, using comprehensive measurements over the rural NCP, is shown in Fig. 9. The calculation method has been described in the Supplement. Unlike HONO and O_3, the photolysis of HCHO directly produces HO_2. Recycling $HO_2 + NO$ contributes to OH formation, while $HO_2 + HO_2$ is the important sink of HO_x in the troposphere. The calculated results show that the OH at the SDZ site can be immediately produced through reaction of $NO + HO_2$, as the production rate of $NO + HO_2$ is remarkably higher than HO_2 loss rate through $HO_2 + HO_2$ (Table S3). Thus, we use HO_x here to represent the OH level. On average, a maximum HO_x production rate ($P[HO_x]$) of 6.5×10^6 molec. cm^{-3} s^{-1} was observed at noon (Fig. 9b). The $P[HO_x]$ could be particularly large during polluted days (Fig. 9a). Figure 10 compares the $P[HO_x]$ during clean days and pollution episodes. The noontime $P[HO_x]$ on polluted days (11.0×10^6 molec. cm^{-3} s^{-1}) was approximately 2 times as large as that on clean days, implying enhanced atmospheric oxidation capacity.

In the conventional view, the photolysis of HONO could provide the major source of OH radical during cold days over the NCP region (Hendrick et al., 2014; Tan et al., 2018). Here we provide the observational evidence of the dominant role of HCHO photolysis in daytime HO_x production in autumn over the rural NCP. The photolysis of HONO was vital in the early morning, but it became less important af-

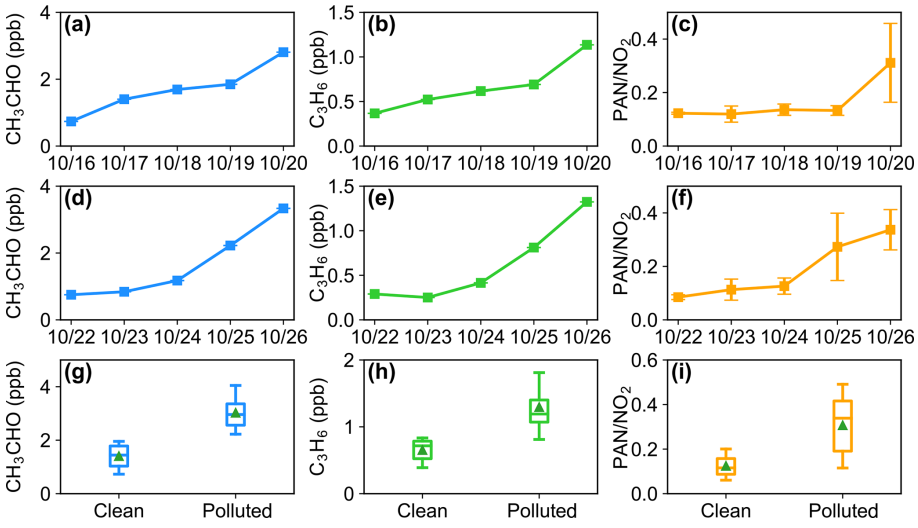

Figure 8. Observed concentrations of CH_3CHO (ppb), C_3H_6 (ppb), and PAN / NO_2 ratios at 08:00 LT **(a–c)** during episode 1 (16–20 October) and **(d–f)** episode 2 (22–26 October) at the SDZ site. **(g–i)** Comparisons between concentrations of CH_3CHO, C_3H_6, and PAN / NO_2 ratios in the mornings on clean days (13–19 and 21–24 October) and polluted days (20 and 25–26 October).

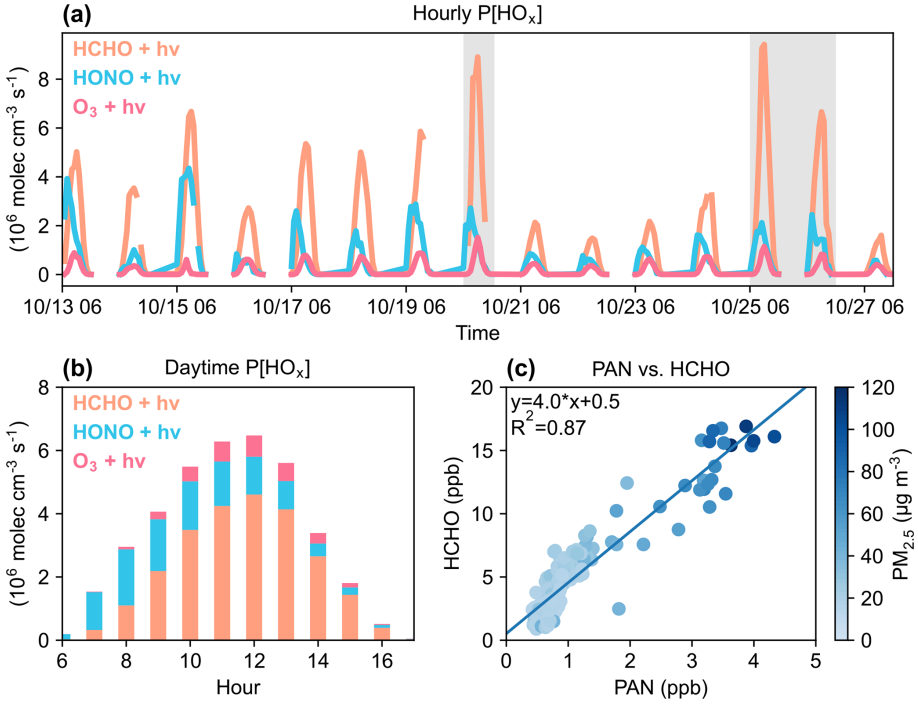

Figure 9. **(a)** Hourly time series of calculated HO_x production rates ($P[HO_x]$) through the photolysis of O_3, HONO, and HCHO during 06:00–17:00 LT from 13 to 27 October at the SDZ site. **(b)** Daytime $P[HO_x]$ through each pathway, averaged over 13–27 October. **(c)** Daytime PAN concentrations versus HCHO concentrations from 13 to 27 October at the SDZ site. The colors denote the corresponding $PM_{2.5}$ levels.

ter 09:00 LT due to its fast decomposition with increasing sunlight (Fig. 9b). On average, the $P[HO_x]$ through HCHO photolysis reached to 4.6×10^6 molec. cm^{-3} s^{-1} at noon, accounting for 71 % among the three pathways (Fig. 9b). During polluted days (20 and 25–26 October), the HCHO photolysis rate reached to 8.3×10^6 molec. cm^{-3} s^{-1} at noon, which was 140 % higher than that on clean days (Fig. 10). Moreover, PAN is strongly correlated with HCHO ($R^2 = 0.87$; Fig. 9c). It proves a similar source of PAN and HCHO, demonstrating the potential impact of HCHO photolysis on

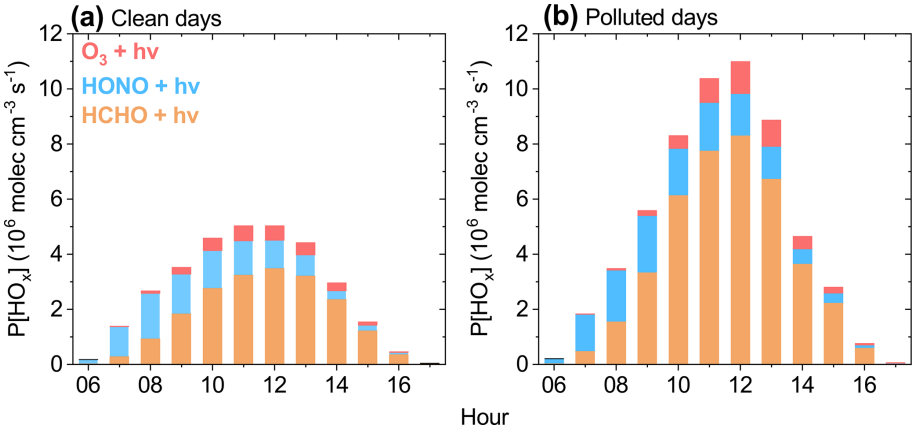

Figure 10. Diurnal variations in $P[HO_x]$ through three pathways during the daytime of clean days (**a**; 13–19 and 21–24 October) and polluted days (**b**; 20, 25, and 26 October) at the SDZ site.

PAN increase at the rural site with accelerated photochemistry. The HO_x sources during cold days have been a subject of recent interest in the field of atmospheric chemistry over the NCP region (Tan et al., 2018; Xue et al., 2020). Using the observation-based box models, most of these studies reported the importance of HONO in the OH radical and atmospheric oxidation capacity during cold days over the NCP. In comparison, our result at the SDZ site presents a much lower HONO concentration (average of 0.15 ppb) than Tan et al. (2018) and Xue et al. (2020). As the SDZ site is located on the northern border of the NCP region, which is much cleaner than the suburban and rural site referenced in Tan et al. (2018) and Xue et al. (2020), and is, thus, less affected by short-live species, such as NO_x and HONO. For another area, Tan et al. (2018) and Xue et al. (2020) conducted measurements during 2016–2017, with HONO concentrations of 0.05–0.98 and 1.8 ppb, while our results were based on observations in the autumn of 2020. The decrease in NO_x emissions during 2016–2020, caused by the strict air pollution control measures since 2013, could explain the observed lower HONO concentration in our study.

HCHO at the SDZ site can be largely affected by aged air masses from the urban NCP region instead of biogenic source because the observed mean concentration of isoprene during polluted days is rather low (0.2 ppb). As shown in Table S4, the observed mean HCHO concentration of 4.6 ± 3.8 ppb at the SDZ site is lower than most observations in urban and suburban Beijing (3.2–29.2 ppb; Pang et al., 2009; Duan et al., 2012; Zhang et al., 2012; Rao et al., 2016; Sheng et al., 2018; Yang et al., 2018; Qian et al., 2019; Zhou et al., 2019) and urban Guangzhou in summer (7.6 ppb; Ling et al., 2017). But it is slightly higher than observations in other southern China areas (2.1–5.6 ppb; Guo et al., 2016; Wang et al., 2017; Yang et al., 2019; P. Zeng et al., 2019) and in the background NCP region (3.5–3.7 ppb) that were conducted 3–6 years before our experiment (Yang et al., 2017; Wang et al., 2020).

4 Discussion and implication

From the results above, we conclude that the substantial increase in PAN at the SDZ site in autumn is a result of local enhanced photochemistry from increased VOC precursor concentrations and HO_x production under a relatively warmer, wetter atmosphere and southerly wind anomalies. In the morning on polluted days, the mean concentration of CH_3CHO is 2.8 times larger than that on clean days. This increase is due to persistent southerly winds, bringing polluted air masses from the urban region to the SDZ site. Besides, the $P[HO_x]$ on polluted days is about 2 times larger than on clean days, owing to the enhanced photolysis of HCHO and HONO. The increases in the CH_3CHO level and $P[HO_x]$ on polluted days could almost explain the enhanced net chemical formation rate (6.3 times that on clean days) with a nearly constant reaction rate coefficient. The accelerated photochemistry by enhanced NO_x and VOCs facilitates the rapid increase in PAN at the background site in autumn.

Unlike previous studies in which HONO was considered as being the key factor of accelerating PAN formation during polluted days (Liu et al., 2018; J. Zhang et al., 2020; Hu et al., 2020), our results demonstrate the dominant role of HCHO photolysis in HO_x production and PAN formation during autumn over the rural NCP region. The enhanced HCHO photolysis on polluted days not only promotes the chemical production of PAN but also accelerates the formation of other secondary pollutants. This is evidenced by the synchronously increased concentrations of PAN, $PM_{2.5}$, and O_3 on polluted days, highlighting the importance of HCHO photolysis from VOC oxidation in secondary pollutant formation under low-NO_x conditions, even during autumn. On the other hand, HCHO itself is also a photochemical product mainly formed through oxidation by NMHCs. Its high level during polluted days and strong correlation with PAN imply the potential role of accelerated photochemistry by enhanced NO_x and VOCs in increases in photochemical pollutants.

The importance of HCHO photolysis on secondary pollutants, as we demonstrated from the SDZ site measurement, could also be applicable to regions with low NO_x emissions but high reactive VOC emissions during cold seasons. The Chinese government has conducted effective NO_x emission controls since 2013 and summertime VOC emission controls in recent years. Our results show that it is also imperative to implement the VOC controls during cold seasons, not just in summer, to avoid the unexpectedly enhanced photochemistry with decreasing NO_x emissions over the NCP region.

5 Conclusion

We performed an integrated observation experiment at a rural site on the northern border of the NCP region in autumn 2020. The observed results show rapid increases in PAN on 2 polluted days, with increasing ratios of 244 % and 178 % over the morning hours (08:00–12:00 LT). Meteorological reanalysis data together with surface observations reveal that southwesterly winds prevail in the NCP during polluted days with a warmer and wetter atmosphere. However, the substantial increases in PAN on polluted days impossibly result from direct PAN transport from the urban region, as the time when the prevailing wind turned to southerly is too late. Using CO as a tracer to exclude the impact of the physical transport of PAN from the urban region, we find that the net chemical formation rates in the morning on polluted days is 0.45 ppb h^{-1}, which is 6.3 times larger than that on clean days. Therefore, the strong local photochemistry could be the main cause of PAN enhancement in the morning on the 2 polluted days.

Further investigation reveals that CH_3CHO oxidation by OH is the major pathway of PA formation at the SDZ site. The C_3H_6 and CH_3CHO concentrations on 16–20 and 22–26 October exhibit increasing trends, demonstrating the cumulative effect and regional transport from the urban region under a meteorological condition of persistent southerly winds during late morning to evening. Statistical results show that the mean CH_3CHO concentration in the morning on polluted days is 2.8 times larger than that on clean days. Additionally, the $P[HO_x]$ on polluted days was about 2 times that during clean days, owing to the enhanced photolysis of HCHO and HONO despite weaker radiation at that time. Consequently, the rapid increase in PAN at the SDZ site in autumn is a result of local enhanced photochemistry from increases in VOC precursor concentrations and HO_x levels. Our study explores the cause of the rapid increase in PAN concentrations at a background site of the NCP region and emphasizes the important role of HCHO in secondary pollutant formation in autumn. It is vital for understanding winter photochemistry under low NO_x emissions.

Data availability. The ERA5 data were accessed from https://doi.org/10.24381/cds.adbb2d47 (Hersbach et al., 2018a) and https://doi.org/10.24381/cds.bd0915c6 (Hersbach et al., 2018b). The observation data for O_x at the MY and urban site were obtained from the Beijing Municipal Ecological and Environmental Monitoring Center (http://www.bjmemc.com.cn/, last access: 6 December 2020). The observation data used in this study can be accessed via https://doi.org/10.7910/DVN/EPAGNB (Qiu and Ma, 2021).

Supplement. The supplement related to this article is available online at: https://doi.org/10.5194/acp-21-17995-2021-supplement.

Author contributions. YQ and ZM designed the study. YQ carried out the analysis and wrote the paper. YQ, ZM, MH, JS, PT, WP, and HZ conducted the observation experiment together. KL, JZ, TH, YT, and HL helped interpret the results. ZM and KL helped to revise this paper.

Competing interests. The contact author has declared that neither they nor their co-authors have any competing interests.

Disclaimer. Publisher's note: Copernicus Publications remains neutral with regard to jurisdictional claims in published maps and institutional affiliations.

Acknowledgements. The authors would like to thank the staff of the Shangdianzi Station for their excellent work. This research has been supported by the Beijing Natural Science Foundation (grant no. 8194078), the open fund by the Jiangsu Key Laboratory of Atmospheric Environment Monitoring and Pollution Control (grant no. KHK2001), and the National Natural Science Foundation of China (grant no. 41475135).

Financial support. This research has been supported by the Beijing Municipal Natural Science Foundation (grant no. 8194078), the National Natural Science Foundation of China (grant no. 41475135), and the Open fund by Jiangsu Key Laboratory of Atmospheric Environment Monitoring and Pollution Control (grant no. KHK2001).

Review statement. This paper was edited by Eleanor Browne and reviewed by three anonymous referees.

References

Alicke, B., Geyer, A., Hofzumahaus, A., Holland, F., Konrad, S., Pätz, H. W., Schäfer, J., Stutz, J., Volz-Thomas, A., and Platt, U.: OH formation by HONO photolysis during the BERLIOZ experiment, J. Geophys. Res.-Atmos., 108, PHO 3-1–PHO 3-17, https://doi.org/10.1029/2001JD000579, 2003.

Chen, Y., Ma, Q., Lin, W., Xu, X., Yao, J., and Gao, W.: Measurement report: Long-term variations in carbon monoxide at a background station in China's Yangtze River Delta region, Atmos. Chem. Phys., 20, 15969–15982, https://doi.org/10.5194/acp-20-15969-2020, 2020.

Dang, R., Liao, H., and Fu, Y.: Quantifying the anthropogenic and meteorological influences on summertime surface ozone in China over 2012–2017, Sci. Total Environ., 754, 142394, https://doi.org/10.1016/j.scitotenv.2020.142394, 2021.

Duan, J., Guo, S., Tan, J., Wang, S., and Chai, F.: Characteristics of atmospheric carbonyls during haze days in Beijing, China, Atmos. Res., 114–115, 17–27, https://doi.org/10.1016/j.atmosres.2012.05.010, 2012.

Edwards, P. M., Brown, S. S., Roberts, J. M., Ahmadov, R., Banta, R. M., deGouw, J. A., Dubé, W. P., Field, R. A., Flynn, J. H., Gilman, J. B., Graus, M., Helmig, D., Koss, A., Langford, A. O., Lefer, B. L., Lerner, B. M., Li, R., Li, S.-M., McKeen, S. A., Murphy, S. M., Parrish, D. D., Senff, C. J., Soltis, J., Stutz, J., Sweeney, C., Thompson, C. R., Trainer, M. K., Tsai, C., Veres, P. R., Washenfelder, R. A., Warneke, C., Wild, R. J., Young, C. J., Yuan, B., and Zamora, R.: High winter ozone pollution from carbonyl photolysis in an oil and gas basin, Nature, 514, 351–354, https://doi.org/10.1038/nature13767, 2014.

Fischer, E. V., Jacob, D. J., Yantosca, R. M., Sulprizio, M. P., Millet, D. B., Mao, J., Paulot, F., Singh, H. B., Roiger, A., Ries, L., Talbot, R. W., Dzepina, K., and Pandey Deolal, S.: Atmospheric peroxyacetyl nitrate (PAN): a global budget and source attribution, Atmos. Chem. Phys., 14, 2679–2698, https://doi.org/10.5194/acp-14-2679-2014, 2014.

Gao, J., Wang, T., Ding, A. J., and Liu, C. B.: Observational study of ozone and carbon monoxide at the summit of mount Tai (1534 m a.s.l.) in central-eastern China, Atmos. Environ., 39, 4779–4791, https://doi.org/10.1016/j.atmosenv.2005.04.030, 2005.

Guo, S., Chen, M., and Tan, J.: Seasonal and diurnal characteristics of atmospheric carbonyls in Nanning, China, Atmos. Res., 169, 46–53, https://doi.org/10.1016/j.atmosres.2015.09.028, 2016.

Hendrick, F., Müller, J.-F., Clémer, K., Wang, P., De Mazière, M., Fayt, C., Gielen, C., Hermans, C., Ma, J. Z., Pinardi, G., Stavrakou, T., Vlemmix, T., and Van Roozendael, M.: Four years of ground-based MAX-DOAS observations of HONO and NO_2 in the Beijing area, Atmos. Chem. Phys., 14, 765–781, https://doi.org/10.5194/acp-14-765-2014, 2014.

Hersbach, H., Bell, B., Berrisford, P., Biavati, G., Horányi, A., Muñoz Sabater, J., Nicolas, J., Peubey, C., Radu, R., Rozum, I., Schepers, D., Simmons, A., Soci, C., Dee, D., and Thépaut, J.-N.: ERA5 hourly data on single levels from 1979 to present, Copernicus Climate Change Service (C3S) Climate Data Store (CDS) [data set], https://doi.org/10.24381/cds.adbb2d47, 2018a.

Hersbach, H., Bell, B., Berrisford, P., Biavati, G., Horányi, A., Muñoz Sabater, J., Nicolas, J., Peubey, C., Radu, R., Rozum, I., Schepers, D., Simmons, A., Soci, C., Dee, D., and Thépaut, J.-N.: ERA5 hourly data on pressure levels from 1979 to present, Copernicus Climate Change Service (C3S) Climate Data Store (CDS) [data set], https://doi.org/10.24381/cds.bd0915c6, 2018b.

Heuss, J. M. and Glasson, W. A.: Hydrocarbon reactivity and eye irritation, Environ. Sci. Technol., 2, 1109–1116, 1968.

Hu, B., Liu, T., Hong, Y., Xu, L., Li, M., Wu, X., Wang, H., Chen, J., and Chen, J.: Characteristics of peroxyacetyl nitrate (PAN) in a coastal city of southeastern China: Photochemical mechanism and pollution process, Sci. Total Environ., 719, 137493, https://doi.org/10.1016/j.scitotenv.2020.137493, 2020.

Kim, S., VandenBoer, T. C., Young, C. J., Riedel, T. P., Thornton, J. A., Swarthout, B., Sive, B., Lerner, B., Gilman, J. B., Warneke, C., Roberts, J. M., Guenther, A., Wagner, N. L., Dubé, W. P., Williams, E., and Brown, S. S.: The primary and recycling sources of OH during the NACHTT-2011 campaign: HONO as an important OH primary source in the wintertime, J. Geophys. Res.-Atmos., 119, 6886–6896, https://doi.org/10.1002/2013JD019784, 2014.

Li, K., Jacob, D. J., Shen, L., Lu, X., De Smedt, I., and Liao, H.: Increases in surface ozone pollution in China from 2013 to 2019: anthropogenic and meteorological influences, Atmos. Chem. Phys., 20, 11423–11433, https://doi.org/10.5194/acp-20-11423-2020, 2020.

Li, K., Jacob, D. J., Liao, H., Qiu, Y., Shen, L., Zhai, S., Bates, K. H., Sulprizio, M. P., Song, S., Lu, X., Zhang, Q., Zheng, B., Zhang, Y., Zhang, J., Lee, H. C., and Kuk S. K.: Ozone pollution in the North China Plain spreading into the late-winter haze season, P. Natl. Acad. Sci., 118, e2015797118, https://doi.org/10.1073/pnas.2015797118 2021.

Ling, Z. H., Zhao, J., Fan, S. J., and Wang, X. M.: Sources of formaldehyde and their contributions to photochemical O_3 formation at an urban site in the Pearl River Delta, southern China, Chemosphere, 168, 1293–1301, https://doi.org/10.1016/j.chemosphere.2016.11.140, 2017.

Liu, L., Wang, X., Chen, J., Xue, L., Wang, W., Wen, L., Li, D., and Chen, T.: Understanding unusually high levels of peroxyacetyl nitrate (PAN) in winter in Urban Jinan, China, J. Environ. Sci., 71, 249–260, https://doi.org/10.1016/j.jes.2018.05.015, 2018.

Liu, J., Liu, Z., Ma, Z., Yang, S., Yao, D., Zhao, S., Hu, B., Tang, G., Sun, J., Cheng, M., Xu, Z., and Wang, Y., Detailed budget analysis of HONO in Beijing, China: Implication on atmosphere oxidation capacity in polluted megacity, Atmos. Environ., 244, 117957, https://doi.org/10.1016/j.atmosenv.2020.117957, 2021.

Liu, Z., Wang, Y., Gu, D., Zhao, C., Huey, L. G., Stickel, R., Liao, J., Shao, M., Zhu, T., Zeng, L., Liu, S.-C., Chang, C.-C., Amoroso, A., and Costabile, F.: Evidence of Reactive Aromatics As a Major Source of Peroxy Acetyl Nitrate over China, Environ. Sci. Technol., 44, 7017–7022, https://doi.org/10.1021/es1007966, 2010.

Lu, K., Fuchs, H., Hofzumahaus, A., Tan, Z., Wang, H., Zhang, L., Schmitt, S. H., Rohrer, F., Bohn, B., Broch, S., Dong, H., Gkatzelis, G. I., Hohaus, T., Holland, F., Li, X., Liu, Y., Liu, Y., Ma, X., Novelli, A., Schlag, P., Shao, M., Wu, Y., Wu, Z., Zeng, L., Hu, M., Kiendler-Scharr, A., Wahner, A., and Zhang, Y.: Fast Photochemistry in Wintertime Haze: Consequences for Pollution Mitigation Strategies, Environ. Sci. Technol., 53, 10676–10684, https://doi.org/10.1021/acs.est.9b02422, 2019.

Lu, X., Zhang, L., Wang, X., Gao, M., Li, K., Zhang, Y., Yue, X., and Zhang, Y.: Rapid Increases in Warm-Season Surface Ozone and Resulting Health Impact in China Since 2013, Environ. Sci. Technol. Lett., 7, 240–247, https://doi.org/10.1021/acs.estlett.0c00171, 2020.

Ma, Z., Xu, J., Quan, W., Zhang, Z., Lin, W., and Xu, X.: Significant increase of surface ozone at a rural site, north of eastern China, Atmos. Chem. Phys., 16, 3969–3977, https://doi.org/10.5194/acp-16-3969-2016, 2016.

Madronich, S., Flocke, S., The role of solar radiation in atmospheric chemistry, in: Handbook of Environmental Chemistry, edited by: Boule, P., Springer-Verlag, Heidelberg, 1–26, 1999.

Pang, X., Mu, Y., Zhang, Y., Lee, X., and Yuan, J.: Contribution of isoprene to formaldehyde and ozone formation based on its oxidation products measurement in Beijing, China, Atmos. Environ., 43, 2142–2147, https://doi.org/10.1016/j.atmosenv.2009.01.022, 2009.

Qian, X., Shen, H., and Chen, Z.: Characterizing summer and winter carbonyl compounds in Beijing atmosphere, Atmos. Environ., 214, 116845, https://doi.org/10.1016/j.atmosenv.2019.116845, 2019.

Qiu, X., Wang, S., Ying, Q., Duan, L., Xing, J., Cao, J., Wu, D., Li, X., Xing, C., Yan, X., Liu, C., and Hao, J.: Importance of Wintertime Anthropogenic Glyoxal and Methylglyoxal Emissions in Beijing and Implications for Secondary Organic Aerosol Formation in Megacities, Environ. Sci. Technol., 54, 11809–11817, https://doi.org/10.1021/acs.est.0c02822, 2020.

Qiu, Y. and Ma, Z.: Replication Data for: Measurement report: Fast photochemical production of peroxyacetyl nitrate (PAN) over the rural North China Plain during haze events in autumn, V2, Harvard Dataverse [data set], https://doi.org/10.7910/DVN/EPAGNB, 2021.

Qiu, Y., Lin, W., Li, K., Chen, L., Yao, Q., Tang, Y., and Ma, Z.: Vertical characteristics of peroxyacetyl nitrate (PAN) from a 250-m tower in northern China during September 2018, Atmos. Environ., 213, 55–63, https://doi.org/10.1016/j.atmosenv.2019.05.066, 2019a.

Qiu, Y., Ma, Z., and Li, K.: A modeling study of the peroxyacetyl nitrate (PAN) during a wintertime haze event in Beijing, China, Sci. Total Environ., 650, 1944–1953, https://doi.org/10.1016/j.scitotenv.2018.09.253, 2019b.

Qiu, Y., Ma, Z., Li, K., Lin, W., Tang, Y., Dong, F., and Liao, H.: Markedly Enhanced Levels of Peroxyacetyl Nitrate (PAN) During COVID-19 in Beijing, Geophys. Res. Lett., 47, e2020GL089623, https://doi.org/10.1029/2020gl089623, 2020a.

Qiu, Y., Ma, Z., Lin, W., Quan, W., Pu, W., Li, Y., Zhou, L., and Shi, Q.: A study of peroxyacetyl nitrate at a rural site in Beijing based on continuous observations from 2015 to 2019 and the WRF-Chem model, Front. Environ. Sci. Eng., 14, 71, https://doi.org/10.1007/s11783-020-1250-0, 2020b.

Rao, Z., Chen, Z., Liang, H., Huang, L., and Huang, D.: Carbonyl compounds over urban Beijing: Concentrations on haze and non-haze days and effects on radical chemistry, Atmos. Environ., 124, 207–216, https://doi.org/10.1016/j.atmosenv.2015.06.050, 2016.

Schnell, R. C., Oltmans, S. J., Neely, R. R., Endres, M. S., Molenar, J. V., and White, A. B.: Rapid photochemical production of ozone at high concentrations in a rural site during winter, Nat. Geosci., 2, 120–122, 2009.

Seinfeld, J. H. and Pandis, S. N.: Atmospheric chemistry and physics: From air pollution to climate change, John Wiley &Sons, Inc., New York, 2006.

Sheng, J., Zhao, D., Ding, D., Li, X., Huang, M., Gao, Y., Quan, J., and Zhang, Q.: Characterizing the level, photochemical reactivity, emission, and source contribution of the volatile organic compounds based on PTR-TOF-MS during winter haze period in Beijing, China, Atmos. Res., 212, 54–63, https://doi.org/10.1016/j.atmosres.2018.05.005, 2018.

Sun, M., Cui, J. N., Zhao, X., and Zhang, J.: Impacts of precursors on peroxyacetyl nitrate (PAN) and relative formation of PAN to ozone in a southwestern megacity of China, Atmos. Environ., 231, 117542, https://doi.org/10.1016/j.atmosenv.2020.117542, 2020.

Tan, Z., Rohrer, F., Lu, K., Ma, X., Bohn, B., Broch, S., Dong, H., Fuchs, H., Gkatzelis, G. I., Hofzumahaus, A., Holland, F., Li, X., Liu, Y., Liu, Y., Novelli, A., Shao, M., Wang, H., Wu, Y., Zeng, L., Hu, M., Kiendler-Scharr, A., Wahner, A., and Zhang, Y.: Wintertime photochemistry in Beijing: observations of RO_x radical concentrations in the North China Plain during the BEST-ONE campaign, Atmos. Chem. Phys., 18, 12391–12411, https://doi.org/10.5194/acp-18-12391-2018, 2018.

Taylor, O. C.: Importance of peroxyacetyl nitrate (PAN) as a phytotoxic air pollutant, Air Repair, 19, 347–351, 1969.

Wang, C., Huang, X.-F., Han, Y., Zhu, B., and He, L.-Y.: Sources and Potential Photochemical Roles of Formaldehyde in an Urban Atmosphere in South China, J. Geophys. Res.-Atmos., 122, 11934–11947, https://doi.org/10.1002/2017JD027266, 2017.

Wang, J., Sun, S., Zhang, C., Xue, C., Liu, P., Zhang, C., Mu, Y., Wu, H., Wang, D., Chen, H., and Chen, J.: The pollution levels, variation characteristics, sources and implications of atmospheric carbonyls in a typical rural area of North China Plain during winter, J. Environ. Sci., 95, 256–265, https://doi.org/10.1016/j.jes.2020.05.003, 2020.

Wang, Y., Hu, B., Tang, G., Ji, D., Zhang, H., Bai, J., Wang, X., and Wang, Y.: Characteristics of ozone and its precursors in Northern China: A comparative study of three sites, Atmos. Res., 132–133, 450–459, https://doi.org/10.1016/j.atmosres.2013.04.005, 2013.

Wei, W., Zang, J., Wang, X., and Cheng, S.: Peroxyacetyl nitrate (PAN) in the border of Beijing, Tianjin and Hebei of China: Concentration, source apportionment and photochemical pollution assessment, Atmos. Res., 246, 105106, https://doi.org/10.1016/j.atmosres.2020.105106, 2020.

Worden, H. M., Deeter, M. N., Frankenberg, C., George, M., Nichitiu, F., Worden, J., Aben, I., Bowman, K. W., Clerbaux, C., Coheur, P. F., de Laat, A. T. J., Detweiler, R., Drummond, J. R., Edwards, D. P., Gille, J. C., Hurtmans, D., Luo, M., Martínez-Alonso, S., Massie, S., Pfister, G., and Warner, J. X.: Decadal record of satellite carbon monoxide observations, Atmos. Chem. Phys., 13, 837–850, https://doi.org/10.5194/acp-13-837-2013, 2013.

Xu, W., Zhang, G., Wang, Y., Tong, S., Ma, Z., Lin, W., Kuang, Y., and Xu, X.: Aerosol Promotes Peroxyacetyl Nitrate Formation During Winter in the North China Plain, Environ. Sci. Technol., 55, 3568–3581, https://doi.org/10.1021/acs.est.0c08157, 2021.

Xu, X., Zhang, H., Lin, W., Wang, Y., Xu, W., and Jia, S.: First simultaneous measurements of peroxyacetyl nitrate (PAN) and ozone at Nam Co in the central Tibetan Plateau: impacts from the PBL evolution and transport processes, Atmos. Chem. Phys., 18, 5199–5217, https://doi.org/10.5194/acp-18-5199-2018, 2018.

Xue, C., Zhang, C., Ye, C., Liu, P., Catoire, V., Krysztofiak, G., Chen, H., Ren, Y., Zhao, X., Wang, J., Zhang, F., Zhang, C., Zhang, J., An, J., Wang, T., Chen, J., Kleffmann, J., Mellouki, A., and Mu, Y.: HONO Budget and Its Role in Nitrate Formation in the Rural North China Plain, Environ. Sci. Technol., 54, 11048–11057, https://doi.org/10.1021/acs.est.0c01832, 2020.

Xue, L., Wang, T., Wang, X., Blake, D. R., Gao, J., Nie, W., Gao, R., Gao, X., Xu, Z., Ding, A., Huang, Y., Lee, S.,

Chen, Y., Wang, S., Chai, F., Zhang, Q., and Wang, W.: On the use of an explicit chemical mechanism to dissect peroxy acetyl nitrate formation, Environ. Pollut., 195, 39–47, https://doi.org/10.1016/j.envpol.2014.08.005, 2014.

Yang, X., Xue, L., Yao, L., Li, Q., Wen, L., Zhu, Y., Chen, T., Wang, X., Yang, L., Wang, T., Lee, S., Chen, J., and Wang, W.: Carbonyl compounds at Mount Tai in the North China Plain: Characteristics, sources, and effects on ozone formation, Atmos. Res., 196, 53–61, https://doi.org/10.1016/j.atmosres.2017.06.005, 2017.

Yang, X., Xue, L., Wang, T., Wang, X., Gao, J., Lee, S., Blake, D. R., Chai, F., and Wang, W.: Observations and Explicit Modeling of Summertime Carbonyl Formation in Beijing: Identification of Key Precursor Species and Their Impact on Atmospheric Oxidation Chemistry, J. Geophys. Res.-Atmos/, 123, 1426–1440, https://doi.org/10.1002/2017JD027403, 2018.

Yang, Z., Cheng, H. R., Wang, Z. W., Peng, J., Zhu, J. X., Lyu, X. P., and Guo, H.: Chemical characteristics of atmospheric carbonyl compounds and source identification of formaldehyde in Wuhan, Central China, Atmos. Res., 228, 95–106, https://doi.org/10.1016/j.atmosres.2019.05.020, 2019.

Zeng, L., Fan, G.-J., Lyu, X., Guo, H., Wang, J.-L., and Yao, D.: Atmospheric fate of peroxyacetyl nitrate in suburban Hong Kong and its impact on local ozone pollution, Environ. Pollut., 252, 1910–1919, https://doi.org/10.1016/j.envpol.2019.06.004, 2019a.

Zeng, P., Lyu, X., Guo, H., Cheng, H., Wang, Z., Liu, X., and Zhang, W.: Spatial variation of sources and photochemistry of formaldehyde in Wuhan, Central China, Atmos. Environ., 214, 116826, https://doi.org/10.1016/j.atmosenv.2019.116826, 2019b.

Zhai, S., Jacob, D. J., Wang, X., Shen, L., Li, K., Zhang, Y., Gui, K., Zhao, T., and Liao, H.: Fine particulate matter ($PM_{2.5}$) trends in China, 2013–2018: separating contributions from anthropogenic emissions and meteorology, Atmos. Chem. Phys., 19, 11031–11041, https://doi.org/10.5194/acp-19-11031-2019, 2019.

Zhang, B., Zhao, B., Zuo, P., Zhi, H., and Zhang, J.: Ambient peroxyacyl nitrate concentration and regional transportation in Beijing, Atmos. Environ., 166, 543–550, https://doi.org/10.1016/j.atmosenv.2017.07.053, 2017.

Zhang, B., Zhao, X., and Zhang, J.: Characteristics of peroxyacetyl nitrate pollution during a 2015 winter haze episode in Beijing, Environ. Pollut., 244, 379–387, https://doi.org/10.1016/j.envpol.2018.10.078, 2019.

Zhang, G., Mu, Y., Zhou, L., Zhang, C., Zhang, Y., Liu, J., Fang, S., and Yao, B.: Summertime distributions of peroxyacetyl nitrate (PAN) and peroxypropionyl nitrate (PPN) in Beijing: Understanding the sources and major sink of PAN, Atmos. Environ., 103, 289–296, https://doi.org/10.1016/j.atmosenv.2014.12.035, 2015.

Zhang, G., Xia, L., Zang, K., Xu, W., Zhang, F., Liang, L., Yao, B., Lin, W., and Mu, Y.: The abundance and interrelationship of atmospheric peroxyacetyl nitrate (PAN), peroxypropionyl nitrate (PPN), O-3, and NOy during the wintertime in Beijing, China, Sci. Total Environ., 718, 137388, https://doi.org/10.1016/j.scitotenv.2020.137388, 2020.

Zhang, H., Xu, X., Lin, W., and Wang, Y.: Wintertime peroxyacetyl nitrate (PAN) in the megacity Beijing: Role of photochemical and meteorological processes, J. Environ. Sci., 26, 83–96, https://doi.org/10.1016/s1001-0742(13)60384-8, 2014.

Zhang, J., Guo, Y., Qu, Y., Chen, Y., Yu, R., Xue, C., Yang, R., Zhang, Q., Liu, X., Mu, Y., Wang, J., Ye, C., Zhao, H., Sun, Q., Wang, Z., and An, J.: Effect of potential HONO sources on peroxyacetyl nitrate (PAN) formation in eastern China in winter, J. Environ. Sci., 94, 81–87, https://doi.org/10.1016/j.jes.2020.03.039, 2020.

Zhang, Y., Mu, Y., Liu, J., and Mellouki, A.: Levels, sources and health risks of carbonyls and BTEX in the ambient air of Beijing, China, J. Environ. Sci., 24, 124–130, https://doi.org/10.1016/S1001-0742(11)60735-3, 2012.

Zhao, X., Gao, T., and Zhang, J.: Heterogeneous reaction of peroxyacetyl nitrate (PAN) on soot, Chemosphere, 177, 339–346, https://doi.org/10.1016/j.chemosphere.2017.03.001, 2017.

Zhou, X., Tan, J., Qin, J., Hu, J., Duan, J., and Chen, R.: Impact of emissions controls on ambient carbonyls during the Asia-Pacific Economic Cooperation summit in Beijing, China, Environ. Sci. Pollut. Res., 26, 11875–11887, https://doi.org/10.1007/s11356-019-04577-5, 2019.

Zhu, H., Gao, T., and Zhang, J.: Wintertime characteristic of peroxyacetyl nitrate in the Chengyu district of southwestern China, Environ. Sci. Pollut. Res., 25, 23143–23156, https://doi.org/10.1007/s11356-018-2412-5, 2018.